Spatial Compounding Algorithm for Speckle Reduction of Dynamic Focus OCT Images

Mohammad R. N. Avanaki, Ramona Cernat, Paul J. Tadrous, Taran Tatla, Adrian Gh. Podoleanu, and S. Ali Hojjatoleslami

***Abstract*— Optical coherence tomography is capable of imaging the microstructures within tissues. To preserve the transverse resolution at all imaging depths, we implement a dynamic focusing scheme. To improve the quality of images further, a simple speckle reduction scheme is employed which uses the vibration introduced by the translation stage used for axial scanning. A spatial compounding technique is developed based on co-registration followed by an averaging algorithm. We conclude that the degree of speckle reduction achieved is worth the expense of more complicated processing required.**

***Index Terms*— Optical coherence tomography, biomedical imaging, spatial compounding, speckle noise reduction.**

I. Introduction

OPTICAL coherence tomography (OCT) is an advanced high resolution, non-invasive imaging modality which delivers three-dimensional (3D) images from translucent microstructures. Time domain OCT (TD-OCT) is the OCT in which different depths are resolved by adjusting the optical path length of the reference arm of an interferometer by using a movable mirror. When the optical path lengths of the light returned from the sample and reference arms match, modulation of the photodetected signal takes place. The signal produced consists of a series of fringes contained ideally within a Gaussian envelope, the width of which defines the depth resolution of the system [1]. The OCT images enable *in-vivo* visualization of structural features of tissue. This is performed noninvasively, with no need to process, section, or stain the tissue. However, the accuracy of diagnosis is marred by a grainy texture that obscures small and low intensity features [2], [3] in the OCT images. When a coherent source illuminates an object, which contains scatterers that are of the same scale or smaller than the central wavelength of the source, the interference of several partial waves produces a phenomenon known as speckle [2]. Development of successful speckle noise reduction algorithms for OCT is particularly challenging. Initially, hardware modifications were employed. Further noise reduction can be achieved by image processing. Some of the most popular image processing methods for speckle reduction are median filtering, adaptive filtering such as homomorphic Wiener filtering, multi-resolution wavelet analysis, adaptive smoothing, soft thresholding using fuzzy systems and lattice filtering [3].

One of the effective ways to reduce the speckle noise is compounding techniques [4]. These techniques are divided into four main categories: spatial-compounding, angular-compounding, polarization-compounding and frequency-compounding. In each of these methods multiple decorrelated frames are averaged. The averaged quantities are: tissue or probe motion for spatial-compounding, beam transmission/receipt angles for angular-compounding, and image formation at different polarizations or frequencies for polarization- or frequency- compounding, respectively.

In this letter, we take advantage of the imperfections in the translation stage used for axial scanning, and applied spatial compounding in order to reduce the speckle noise. Although, the method is applicable to any OCT system uses a moving element in the sample arm.

II. Dynamic Focus OCT Configuration

The OCT system employed for imaging in this letter is an *en-Face* time domain OCT which uses a dynamic focusing (DF) scheme. The sample arm of such system is shown in Fig. 1. The details of the design and implementation of the DF-OCT are given in [5]. With conventional OCT, the confocal gate is stationary and the reference arm moves the coherence gate to scan the confocal gate. In this scheme, the coherence gate is synchronized with the peak of confocal gate profile. Hence, the transverse resolution is preserved throughout the full imaging depth and an enhanced signal is returned from all depths. The system operates at 1300 nm and uses a super luminescent diode (SLD) with a 3 dB spectral bandwidth of 54 nm. The dynamic focus allows better penetration, as demonstrated in previous studies of basal cell carcinoma [8]. DF-OCT removes the need for deconvolution of axial reflectivity profiles with the confocal gate profile [9], [10]. More details on the advantages of such a DF-OCT system can be found in [5].

Manuscript received September 4, 2012; revised March 21, 2013; accepted May 2, 2013. Date of publication June 12, 2013; date of current version July 9, 2013. This work was supported by the National Institute for Health Research (NIHR) i4i programme. The views expressed are those of the author(s) and not necessarily those of the NHS, the NIHR, or the Department of Health. The work of A. Gh. Podoleanu was supported by the ERC 249889 and by the NIHR Biomedical Research Centre at Moorfields Eye Hospital NHS Foundation Trust and UCL Institute of Ophthalmology.

M. R. N. Avanaki and S. A. Hojjatoleslami are with Neurosciences and Medical Image Computing Group, University of Kent, Canterbury CT2 7PD, U.K. (e-mail: mn96@kent.ac.uk; S.A.Hojjatoleslami@kent.ac.uk).

R. Cernat and A. Gh. Podeleanu are with Applied Optics Group, School of Physical Sciences, University of Kent, Canterbury CT5 3EX, U.K. (e-mail: A.G.H.Podoleanu@kent.ac.uk).

P. J. Tadrous is with the Department of Cellular Pathology, Northwick Park Hospital, London HA1 3UJ, U.K.

T. Tatla is with the ENT-H&N Surgery, Northwick Park Hospital, London HA1 3UJ, U.K.

Color versions of one or more of the figures in this letter are available online at http://ieeexplore.ieee.org.

Digital Object Identifier 10.1109/LPT.2013.2266660

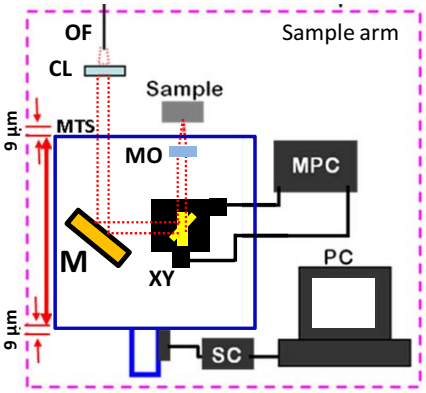

Fig. 1. Schematic of the sample arm of the dynamic focus OCT system. PC: personal computer, CL: collimation lens, M: flat mirror, XY: orthogonal galvo-scanners, MO: microscope objective, MPC: mirror positioning controller, SC: stage controller, MTS: motorised translation stage, OF: optical fiber.

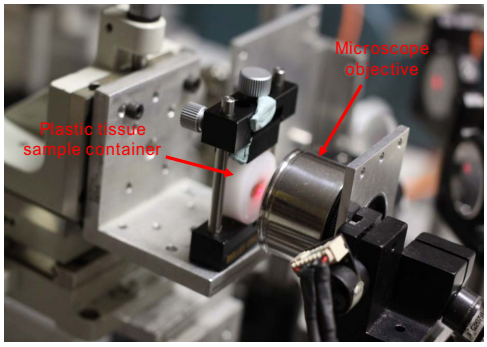

Fig. 2. Demonstration of how the plastic container including the larynx tissue sample and the microscope objective are located in front of the lens (MO in Fig 1) moving together with the MTS.

Larynx tissue samples (*ex-vivo*) were used as imaging targets. The larynx tissues were excised from a patient at Northwick Park Hospital, UK, stained with haematoxylin and eosin, and placed into a small PVC cylinder (2 cm diameter × 1 cm height) closed at both ends by glass coverslips 180 micron thick and further sealed with a layer of high vacuum silicone grease between the plastic and the coverslip. 10% formalin solution filled the cylinder. The tissue sample container is mounted on the sample holder 7.5 mm away from the surface of the objective lens (Fig. 2); this is the working distance of the objective microscope lens.

III. Spatial Compounding Algorithms

The translation stage used to collect the B-scan images is not perfect. Each time the stage moves forward or backward, a displacement error of up to 20 μm occurs in addition to the desired displacement (see Fig. 1). Thus, despite targeting a specific region in the sample, a region axially shifted by few microns is actually imaged. We let the translation stage work in different experiments while recording the actual position of the translation stage via the stage controller (ESP300, Newport corp). Via these measurements, we obtained the displacement error in more than 800 different measurements in different experiments. In all of these experiments, the imaging depth was set to 1 mm. It was found that the displacement error follows a Gaussian distribution with a mean distribution of

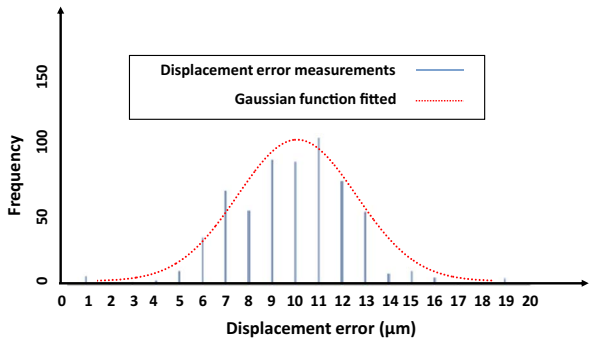

Fig. 3. Displacement error of the translation stage.

9 μm over a 1 mm imaging depth range (see Fig. 3). For an axial range of 1.7 mm and an image made from 342 T-scan lines, the axial size of the pixel in the image is 5 μm. This suggests that the unintentional displacement of the translation stage can shift the intensity value of a pixel in the B-scan image axially by up to two pixels.

After acquiring B-scan images from a specimen, the location of high gradient pixels in the image is detected as a landmark to co-register the images. A Sobel edge detector is used to detect such landmarks followed by a spatial median filter [6], [7]. Then all the images are truncated from this landmark. Five different speckle reduction algorithms were evaluated in this letter.

Averaging: the corresponding pixels to a pixel location are averaged.

Median Filtering (MF): the corresponding pixel value to a pixel location are sorted in ascending order. Sorting the pixels here and in all the other following methods is along the batch. The median value is then calculated and substituted with the pixel value.

Random Weighted Averaging (RWA): the value of every pixel in the image is multiplied by a random number between 0 to 5. This procedure is repeated for all the pixel values of the images. It is assured that amongst the pixels corresponding to a pixel location, there is at least one pixel that has a modulation between 1 and 5. The corresponding pixels to the pixel location are then averaged.

Random Pixel Selection (RPS): the corresponding pixels to a pixel location are stored and one of them is chosen randomly to represent the value of the pixel. This procedure is repeated for every pixel location across the image.

Random Pixel Selection + Median Filtering (RPS+Median): this is similar to the procedure described in RPS above, followed by a two dimensional 3×3 median filter.

IV. Results and Discussions

The algorithms were implemented in Matlab 2011. For evaluation purposes, 60 B-scan images were acquired from the larynx tissue samples. The results of applying the algorithm on the images are shown in Fig. 4. Also we have compared our results to that of our previously proposed method [11]. In this method, the noise is modeled using Rayleigh distribution with a noise parameter σ to be estimated by an artificial neural network (ANN). The estimated σ is then used along

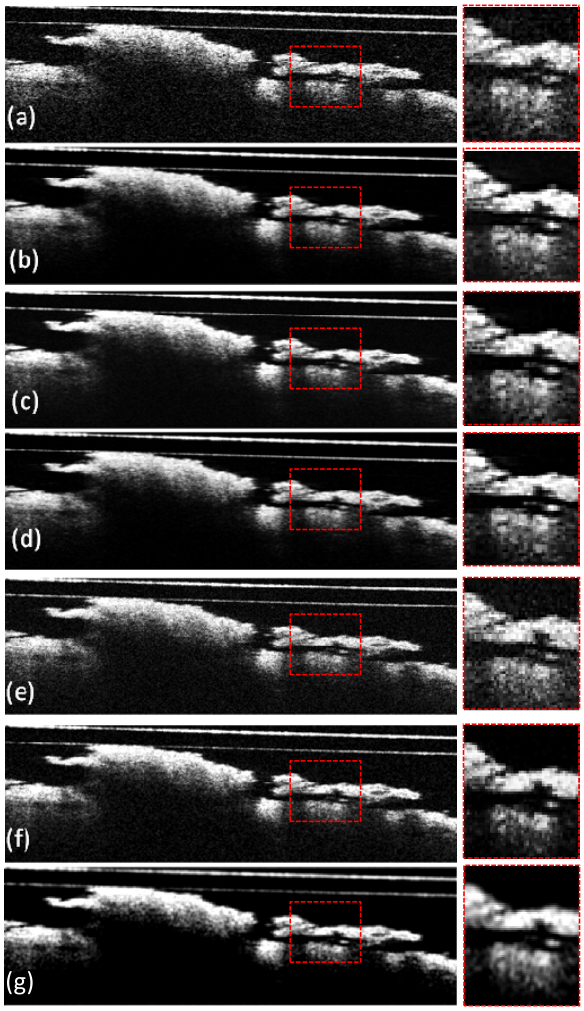

Fig. 4. Results of the speckle reduction algorithms applied to 60 B-scan images of a larynx sample acquired by the DF-OCT system. Size of the images is 2.25 mm × 1 mm. (a) Original image, improved images using (b) averaging, (c) median filtering, (d) random weighted averaging, (e) random pixel selection, (f) random pixel selection followed by a 3×3 two dimensional median filtering, (g) artificial neural network method.

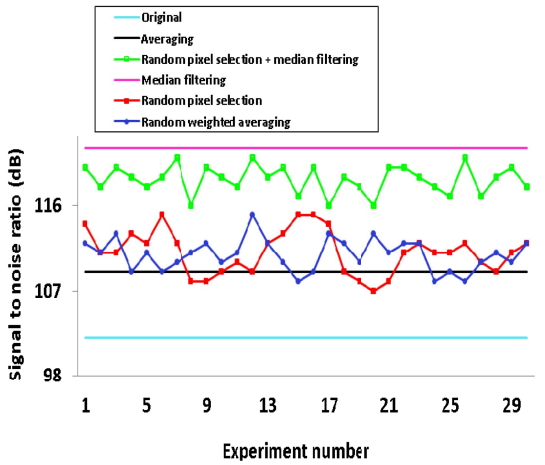

Fig. 5. Calculation of SNR for the images in Fig 4.

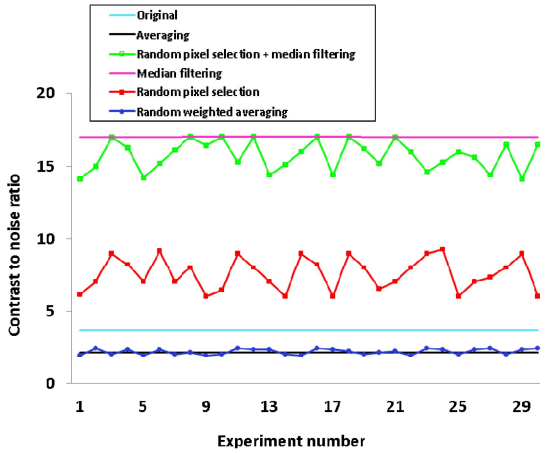

Fig. 6. Calculation of CNR for the images in Fig. 4.

with the inverse Rayleigh function to reduce the noise in the image. The obtained image from this method is shown in Fig. 4(g).

To evaluate the reliability of the probabilistic algorithms, each algorithm was applied 30 times on the same region of the images. Improvement in the quality of the images is noted by visual inspection. Among the algorithms, the median filtering and RPS + median produced images with slightly better contrast. The SNR was used as a quantitative metric to evaluate the improvement in the images due to the speckle reduction [3]. SNR measures the strength of an object in the image in the presence of the background noise:

$$SNR = 10\log_{10}(\max\{B_{lin}^2\}/\sigma_{lin}^2) \tag{1}$$

where B_{lin}^2 is the linear magnitude image, and σ_{lin}^2 is the variance of B_{lin}^2 in a background noise. The SNR calculated for the images are shown in Fig. 5. We have calculated the SNR for 10 homogeneous regions in each image, then averaged them. We have also evaluated the images using the contrast-to-noise ratio (CNR) [3].

$$CNR = \frac{1}{R}\left(\sum_{r=1}^{R}\frac{(\mu_r - \mu_b)}{\sqrt{\sigma_r^2 + \sigma_b^2}}\right) \tag{2}$$

where μ_b and σ_b^2 in CNR represent the mean and variance of the same background noise region, and μ_r and σ_r^2 represent the mean and variance of the r_{th} region of interest respectively [3]. In line with other published work [3], we used 5 regions (R=5) in the calculation of CNR. The CNR calculated for the images are shown in Fig. 6.

To further illustrate the effect of the filters on the edges, in Fig. 7, A-line intensity profile (for the part of the image indicated with a red dotted box inside Fig. 7), are compared. The A-lines are averaged horizontally within the red dotted box. Each of the random-weighted and random pixel selection algorithms were repeated 30 times on the same region to evaluate the variation of SNR and CNR. For the deterministic algorithms, however, the SNR and CNR are constant. Among the five algorithms tested, median filtering produced images with the largest SNR and best visual contrast. This is consistent with the fact that the median of several intensity values corresponding to a pixel location is the most probable intensity value of that location. The SNR of the images produced by the

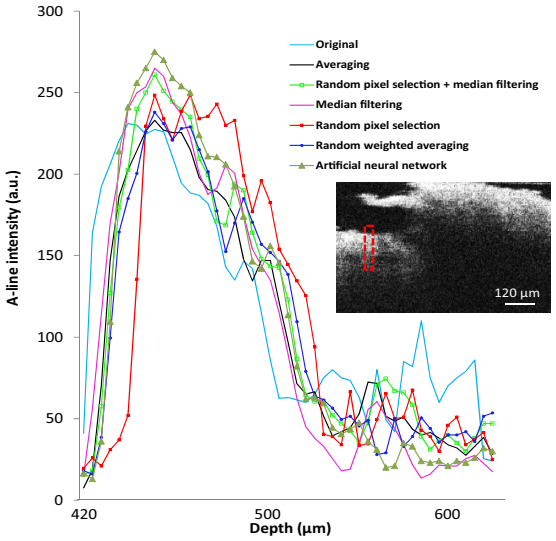

Fig. 7. Results for the A-line improvement. The A-lines are averaged horizontally within the red dotted box.

random pixel selection method were inferior to those produced by median filtering. The 3×3 pixel median filter was applied to the resultant image of the random pixel selection method in order to eliminate the remaining salt and pepper noise on the images. The size of the median filter was determined by optimization to achieve a larger SNR and reduce the blurriness of the image.

Compared to the commonly used speckle reduction method, based on simple averaging, the spatial compounding technique based on median filtering method and the RPS + median method were found to be more efficient from quantitative and qualitative point of views, respectively. The SNR calculated for the ANN method was 125 dB which suggests that the proposed algorithms can reduce the noise to a great extent, although not as much as the ANN or any comparable speckle reduction algorithm can do. The spatial compounding technique with the algorithms introduced above have also been successfully tested on the images of healthy and Basaloid skin, as well as phantoms and resulted in significant improvement in the contrast and SNR of the images.

The algorithms were tested on a 2.2 GHz Pentium IV computer with 4GB memory. Comparing the time that the ANN method requires for training which is in order of minutes to that of the millisecond order of the algorithms proposed here, shows the efficiency of the algorithms evaluated here.

The method presented can in principle be used for speckle reduction in all OCT systems employing imperfect axial moving element in the sample arm, where the error in axial positioning, smaller than the coherence length, can be used as a modulating factor of the speckle. In cases where the sample under investigation is stationary, the spatial compounding represents a much lower cost solution than any other hardware methods reported.

V. Conclusion

A spatial compounding technique for speckle reduction is proposed for those OCT systems utilizing imperfect axial scanners. The algorithm presented is based on finding the most likely intensity value for each pixel at a specific location in the image. Evaluation of the images acquired showed sufficient qualitative improvement.

The algorithms were tested on a dynamic focus OCT. Despite lower acquisition speed, the DF-OCT implementation may find niche applications in the OCT investigation of samples where acquisition speed is not a problem and a transversal resolution in the range of microns is necessary. Moreover, although the algorithms were tested on a TD-OCT, they can be applied on the images acquired with any type of OCT that has a moving element in the sample arm. The algorithm may however change according to the type of displacement error.

Acknowledgment

The authors would like to thank Dr. T. Ju for his comments and help.

References

[1] A. G. Podoleanu, "Optical coherence tomography," *Brit. J. Radiol.*, vol. 78, pp. 976–988, Nov. 2005.

[2] J. W. Goodman, *Speckle Phenomena in Optics: Theory and Applications*. Englewood, CO, USA: Roberts & Co, 2006.

[3] A. Ozcan, A. Bilenca, A. E. Desjardins, B. E. Bouma, and G. J. Tearney, "Speckle reduction in optical coherence tomography images using digital filtering," *J. Opt. Soc. Amer. A*, vol. 20, no. 7, pp. 1901–1910, 2007.

[4] P. Shankar, "Speckle reduction in ultrasound B-scans using weighted averaging in spatial compounding," *IEEE Trans. Ultrason. Ferroelectr. Freq. Control*, vol. 33, no. 6, pp. 754–758, Nov. 1986.

[5] M. Hughes and A. G. Podoleanu, "Simplified dynamic focus method for time domain OCT," *Electron. Lett.*, vol. 45, no. 12, pp. 623–624, 2009.

[6] M. R. N. Avanaki and A. Hojjat, "Speckle reduction with attenuation compensation for skin OCT images enhancement," in *Proc. Int. Conf. Med. Image Understand. Anal.*, 2009, pp. 123–128.

[7] A. Hojjatoleslami and M. R. Nasiriavanaki, "OCT skin image enhancement through attenuation compensation," *App. Opt. J.*, vol. 51, no. 21, pp. 4927–4935, 2012.

[8] M. R. N. Avanaki, A. Hojjatoleslami, M. Sira, J. B. Schofield, C. Jones, and A. G. Podoleanu, "Investigation of basal cell carcinoma using dynamic focus optical coherence tomography," *Appl. Opt.*, vol. 52, no. 10, pp. 2116–2124, 2013.

[9] M. Avanaki, *et al.*, "Quantitative evaluation of scattering in optical coherence tomography skin images using the extended Huygens-Fresnel theorem," *Appl. Opt.*, vol. 52, no. 8, pp. 1574–1580, 2013.

[10] D. Levitz, *et al.*, "Determination of optical scattering properties of highly-scattering media in optical coherence tomography images," *Opt. Express*, vol. 12, no. 2, pp. 249–259, 2004.

[11] M. R. N. Avanaki, P. P. Laissue, A. G. Podoleanu, and A. Hojjat, "Denoising based on noise parameter estimation in speckled OCT images using neural network," *Proc. SPIE*, vol. 7139, p. 71390E, Sep. 2008.

[12] M. Avanaki, "Image enhancement algorithms and system optimization for optical coherence tomography," Ph.D. dissertation, School Biosci., Univ. Kent, Canterbury, U.K., 2011.